BOREAS An international journal of Quaternary research

A 1286-year hydro-climate reconstruction for the Balkan Peninsula

LARA KLIPPEL, PAUL J. KRUSIC, ROBERT BRANDES, CLAUDIA HARTL, SOUMAYA BELMECHERI, MANUEL DIENST AND JAN ESPER

BOREAS

Klippel, L., Krusic, P. J., Brandes, R., Hartl, C., Belmecheri, S., Dienst, M. & Esper, J.: A 1286-year hydro-climate reconstruction for the Balkan Peninsula. *Boreas*. https://doi.org/10.1111/bor.12320. ISSN 0300-9483.

We present a June–July drought reconstruction based on the standardized precipitation index (SPI) for the Balkan Peninsula over the period 730–2015 CE. The reconstruction is developed using a composite *Pinus heldreichii* tree-ring width chronology, from a high-elevation network of eight sites in the Pindus Mountains in northwest Greece, composed of living trees and relict wood. The dataset includes the ring width series of Europe's currently oldest known living tree, dendrochronologically dated to be more than 1075 years old. The spatial coverage of the reconstruction is improved by using an averaged gridded SPI data target derived from a response field that is located north of the study region. Justification for this approach includes the remoteness of instrumental data, the spatial variability of precipitation and synoptic scale circulation patterns. Over the past 1286 years, there have been 51 dry and 43 pluvial events. The driest year during the 1286-year-long period was 1660 and the wettest year was 1482. Comparison with shorter reconstructions and documentary evidence validates the new reconstruction, and provides additional insight into socioeconomic impacts and spatial patterns of extreme events. Fifty-nine of 72 previously undescribed extremes occurred prior to the 17th century. The new reconstruction reveals long-term changes in the number of extremes, including substantially fewer drought and pluvial events in the 20th century. Additional tests on the long-term effects of age structure, replication and covariance changes support the heteroscedastic nature of the reconstructed hydro-climatic extremes.

Lara Klippel (L.Klippel@geo.uni-mainz.de), Claudia Hartl, Manuel Dienst and Jan Esper, Department of Geography, Johannes Gutenberg University, Mainz 55099, Germany; Paul J. Krusic, Department of Geography, University of Cambridge, Cambridge CB23EN, UK; Navarino Environmental Observatory, Messina, Greece; and Department of Physical Geography, Stockholm University, Stockholm, Sweden; Robert Brandes, Department of Geography, Friedrich-Alexander University Nürnberg-Erlangen, Erlangen 91058, Germany; Soumaya Belmecheri, Laboratory of Tree-Ring Research, University of Arizona, Tucson, AZ 85721, USA; *received 2nd February 2018, accepted 5th April 2018.*

Across the Mediterranean climate models predict, in forthcoming decades, a summer temperature increase and a summer precipitation reduction (Giorgi & Lionello 2008; Diffenbaugh & Giorgi 2012). In terms of spatial distribution, the largest temperature increase is expected for the Iberian and Balkan Peninsulas (Dubrovský *et al.* 2013), accompanied by an amplification in the frequency, intensity and duration of summer droughts (Gao & Giorgi 2008) and heatwaves (Fischer & Schar 2010; Nastos & Kapsomenakis 2015). Meteorological records reveal a precipitation decrease in recent decades in the eastern Mediterranean (Maheras & Anagnostopoulou 2003; García-Herrera *et al.* 2007), and extreme drought episodes have become more frequent and persistent (Xoplaki *et al.* 2004). To place the recent and predicted conditions in a long-term context, palaeoclimate reconstructions are needed (Esper *et al.* 2007; Schneider *et al.* 2015; Ljungqvist *et al.* 2016; Wilson *et al.* 2016).

Along the Balkan Peninsula, including the Pindus Mountain range in Greece, we find very old *Pinus heldreichii* (PIHE; Brandes 2007) stands with several individuals reaching millennial age. The oldest individual, named *Adonis*, is dendrochronologically dated to be over 1075 years old (Konter *et al.* 2017). This makes it currently the oldest known living tree in Europe, and provides a history of climatic and environmental conditions going back into the first millennium. This long-lived species has been used in several dendrochronological studies (e.g. Todaro *et al.* 2007; Panayotov *et al.* 2010; Seim *et al.* 2012; Trouet *et al.* 2012; Klesse *et al.* 2015). Recent studies relying on maximum latewood density have successfully reconstructed past temperature variations using PIHE (Trouet *et al.* 2012; Klesse *et al.* 2015), but there has been no attempt yet to reconstruct changes in past climate by means of total tree-ring width (TRW) measurements. It has been shown that the low frequency climate signal in TRW measurements is not stable (Seim *et al.* 2012), although at higher frequencies temperature and precipitation have significant growth implications (Klippel *et al.* 2017). PIHE growth at Mt Smolikas is significantly controlled by temperature in April and precipitation in June–July, which emphasizes the overall importance of an early growth onset and subsequent moisture conditions (Klippel *et al.* 2017).

There are several high-resolution reconstructions of hydro-climatic conditions from the eastern Mediterranean, derived from TRW of other species, e.g. *Juniperus excelsa* (Touchan *et al.* 2005), *Pinus nigra* (Akkemik & Aras 2005; Köse *et al.* 2011; Levanic *et al.* 2012; Poljanšek *et al.* 2013; Klesse *et al.* 2015) and *Quercus* sp. (Akkemik *et al.* 2005; Griggs *et al.* 2007; Cufar *et al.* 2008). However, our understanding of the spatiotemporal patterns and magnitude of precipitation changes, particularly prior to the Little Ice Age (LIA), is still limited due to an increasing data paucity back in time (Esper *et al.* 2016). Based on the stable climate signal in the high-frequency domain, this work aims to develop for the first time a PIHE TRW based summer precipitation reconstruction extending back to the first millennium. We focus on interannual variability in

DOI 10.1111/bor.12320

hydro-climate and the identification of extreme dry and pluvial events.

Data and methods

Study area and tree-ring data

Tree-ring data used in this study comprise 207 821 annual ring width measurements, from 133 relict and 185 living PIHE trees, sampled between the years 2011 and 2016. We compiled a composite TRW chronology from eight different locations (Table 1) in the timberline ecotone of Mt Smolikas at 1950–2200 m a.s.l. (the highest peak of the Pindus Range in northern Greece; Fig. 1A). Conditions, such as rocky shallow soils, summer dryness, snow cover in winter (Fotiadi *et al.* 1999; Loukas *et al.* 2002) and decay resistant resinous wood (Lange *et al.* 1994), permit the preservation of relict material. PIHE is native to the oro-mediterranean vegetation belt (Brandes 2007), a region characterized by large seasonal temperature and precipitation changes, including heavy winter frosts and snow, and intense dryness during the summer period (Bolle 2003).

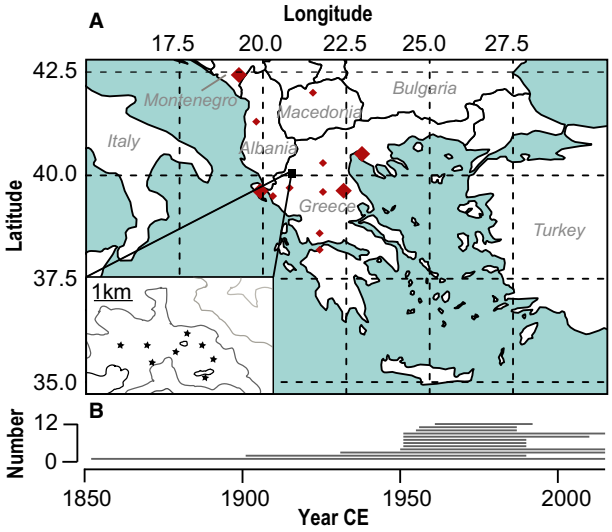

Fig. 1. Site characteristics. A. Location of the study area in the Pindus Mountains (black square) and map of the sampling sites at the eastern flank of Mt Smolikas (inset). Red symbols refer to the climate stations used for interpolation of the closest CRU TS3.24.01 precipitation grid (40.25°N/20.75°E). Large/small red diamonds indicate currently active/inactive climate stations. B. Temporal coverage of instrumental station measurements. From top to bottom, lines refer to the climate stations in Skopje, Agrinion, Kozani, Petgorica-Grad, Tirana, Trikala, Igoumenitsa, Ioannina, Larissa, Thessaloniki, Patrai and Kerkyra.

Tree-ring measurement and chronology development

Six hundred fifteen discs and core samples were prepared following standard dendrochronological techniques to produce finely polished surfaces for micrometre measurement. TRW was measured using the Velmex and Lintab systems, TSAP-Win (Rinn 2003) and Cofecha programs (Holmes 1983). To emphasize varying frequencies in the TRW chronologies, age-related trends (Bräker 1981) were removed by applying two different detrending procedures to power-transformed TRW series (Cook & Peters 1997). To remove age trends in the individual tree-ring series, and to preserve common frequency signals, a regional curve standardization (RCS; Briffa *et al.* 1992; Cook & Peters 1997; Esper *et al.* 2003) was performed in order to produce a chronology retaining low-frequency variance, and individual cubic smoothing spline (SPL) standardization, with a 50% frequency cut-off at 2/3 of the series length, was applied to preserve climatic information at annual-to-multidecadal scales (Cook & Peters 1997). Both chronologies were produced using the option configurations within the program ARSTAN (Cook *et al.* 2017). RCS allows climatic information to be preserved on time scales longer than the individual segment length and long-term changes in environmental conditions are preserved (Cook *et al.* 1995). Ideally, RCS is applied to composite datasets integrating living and relict material with a heterogeneous age structure (Esper *et al.* 2003). The application of RCS to this dataset is limited, as samples from very old and slow-growing living trees are combined with relict samples that are heavily weath-

Table 1. Characteristics of the individual site and Mt Smolikas regional (all) chronologies. EPS = expressed population signal; MSL = mean segment length; AGR = average growth rate (mm) of the first 300 years of growth; Lag1 = first-order autocorrelation; Rbar = inter-series correlation.

Site	Elevation	Exposure	n series	Start (EPS >0.85)	End	MSL	AGR	Lag1	Rbar
1	2141	NW	152	673 (980)	2015	394	0.82	0.77	0.31
2	2163	S	111	575 (1345)	2014	316	0.77	0.75	0.34
3	1951	N	98	720 (1555)	2015	320	0.79	0.76	0.32
4	2070	NE	99	685 (1500)	2014	308	0.78	0.77	0.42
5	2091	SE	60	1072 (1500)	2015	293	0.87	0.82	0.30
6	2209	S	43	1167 (1605)	2015	345	0.78	0.79	0.31
7	2103	SE	29	1172 (1630)	2015	359	1.08	0.82	0.40
8	2049	NW	23	1493 (1650)	2015	351	1.15	0.77	0.27
All	2097		615	575 (730)	2015	338	0.82	0.77	0.31

ered and of shorter and mixed ages. Amongst all the individual TRW series, common variability over time was assessed using inter-series correlation (Rbar) and expressed population signal (EPS; Wigley *et al.* 1984) calculated over 30-year periods with 15 years of overlap. High inter-series correlation as well as common inter-site growth and climate response patterns (Klippel *et al.* 2017) permitted the establishment of a composite chronology including all samples. The composite chronology was formed by calculating the robust bi-weight mean of the RCS tree-ring indices of each calendar year, truncated at EPS >0.85 (Cook 1985). Based on the number of samples and Rbar, variance stabilization was applied (Frank *et al.* 2007b). To investigate high-frequency changes, we used the (pre-whitened) residual version of the chronology, produced by removing common persistence by autoregressive modelling (Cook 1985).

Heteroscedasticity tests

The correct detection of extreme events requires that all preserved variance changes have a climatic origin and do not arise from biological and methodological artefacts (Fritts 1976). Any systematic trend in variance, in the individual series and/or chronology, could potentially bias the calculation of the tree-ring chronology. Raw ring width series are heteroscedastic by nature. Prior to detrending, the power transformation of the raw measurements minimizes age-dependent shifts in variance of non-climatic origin, by suspending the growth level vs. spread relationship (Cook & Peters 1997). In the composite chronology, changes over time in the inter-series correlation and sample replication are another source of potential variance bias. According to Frank *et al.* (2007b), the process of variance stabilization attempts to remove variance changes related to replication and inter-tree correlation, while it preserves variance related to climate. To assess these effects over the past millennium, variance changes in the SPL chronology were analysed by calculating 100-year moving window standard deviations (SDs). We account for the effect of (i) sample replication and explore (ii) the age-structure of the dataset as potential drivers for non-climatic variance changes as follows:

- Additional tests for remaining biases due to temporal variations of replication in the mean chronology were conducted by subsampling the residual SPL chronology to produce a suite of new residual chronologies with a time-invariant replication. In the first step, from the total of 615 residual series (Fig. S1A), 1000 subsample residual series, spanning the period 730–2015, were generated by randomly new composition of the individual series (Fig. S1B). In the second step, 1000 times 80 of these series were randomly selected and averaged into a subset chronology with a balanced yearly sample size (Fig. S1C). The second step was repeated using only 15 series, which is the minimum replication of the original chronology.
- The age-dependency of variance was explored by analysing the spread of individual cambial age-aligned residual series. Tests for remaining bias due to a temporally changing age-structure were conducted by splitting the dataset into different age classes. Age-class chronologies range from 1–200 years, and 201–400 years. Additionally, an arithmetic mean chronology of the two age-class chronologies, 1–200 and 201–400, was created, balancing the age structure of the dataset through time.

Instrumental data

Existing instrumental climate data, predominantly from distant low elevation sites, probably underestimate precipitation and overestimate temperature of the study area (Fig. 1A). Due to the poor ability of local station data to capture climatic conditions at the upper tree line, we considered high-resolution 0.5° gridded CRU TS 3.24 climate data (Harris *et al.* 2014) to assess the temporal stability and spatial extent of the TRW climate signal. To exclude potential uncertainty in gridded data, calibration/verification tests were performed over the 1961–2015 period resulting from the limited number of reliable instrumental station records during the first half of the 20th century (Fig. 1B). Using the interpolated CRU TS 3.24 precipitation data for each grid cell within 15–50°E and 34–50°N, we calculated the standardized precipitation index (SPI; McKee *et al.* 1993). SPI was chosen as the index because it has been identified as an effective metric for detecting dry and pluvial events in Mediterranean pine forests and is widely used to investigate meteorological drought on a range of time scales (Pasho *et al.* 2011; Levanic *et al.* 2012; Seftigen *et al.* 2013; Tejedor *et al.* 2016). Standardized precipitation is the deviation of rainfall totals over a defined time interval (in this study: 1-month and 2-month) from the average precipitation over the entire record divided by its standard deviation (McKee *et al.* 1993). The SPI value can be interpreted as the number of standard deviations by which the defined time interval deviates from the long-term mean. A normalized expression of precipitation enables cross-region comparisons of pluvial and drought conditions (McKee *et al.* 1993). The SPL residual, SPL standard and RCS chronologies were first calibrated against the 1-month and 2-month SPI, temperature and precipitation using the closest grid point at 20.5–21°E/40–40.5°N. To investigate the spatial extent of the signal with the strongest response, the procedure was repeated using all 0.5° grids within 15–50°E and 34–50°N. The average SPI of all grid points correlating at a p-value ≤ 0.001 during the most important season/month was considered for further calibration and verification tests.

SPI reconstruction and determination of extreme events

A linear model was established to explain the relationship between the regional SPL residual chronology and SPI. A split calibration/verification approach was used to estimate the reliability and predictive power of the transfer function over time. The explained variance (r^2), reduction of error statistic (RE, Briffa *et al.* 1988), coefficient of efficiency (CE, Cook *et al.* 1994) and the Durbin–Watson test (DW, Durbin & Watson 1951) were used to estimate the robustness of the final model. Positive RE and CE scores indicate the reconstruction skill of the model (Cook *et al.* 1994). The DW statistic tests for autocorrelation in the model residuals. A DW value of 2 suggests little to no autocorrelation, whereas smaller (larger) values indicate positive (negative) autocorrelations, respectively. Two-tailed 95% confidence intervals were computed using a Monte Carlo approach to account for model uncertainty. In the first step, this procedure includes the random generation (n = 1000) of time series of the response variable SPI for the period 1961–2015 with an amount of variance equal to the residual standard error of the model. In the second step, we repeated the procedure of linear modelling using the 1000 series to establish SPI estimates based on TRW. For the detection of extremely dry and pluvial events, we adopted the threshold of ±1 SD (McKee *et al.* 1993). The final reconstruction was transferred using linear regression instead of a scaling to support the estimation of uncertainty due to unexplained instrumental SPI variance (Esper *et al.* 2005). All analysis was performed using the R software (R Core Team 2017).

Results

Chronology characteristics and heteroscedasticity

By combining 615 living and dead wood series, we produced a chronology that covers the period 575–2015 CE (730–2015 CE, EPS >0.85; Fig. 2A, B). The longest series from the living tree *Adonis* contains 1075 rings, and the longest relict series covering 873–1737 CE has 865 rings. Sample replication decreases from 329 series in 2014 to 146 series in 1500, 43 series in 1000, and 15 series in 730 (Fig. 2C). Mean Rbar is 0.31 (Fig. 2D) and first-order autocorrelation is 0.77 (Table 1). Comparison of the SPL and RCS techniques clearly demonstrates that the RCS chronology captures longer-term variability, including multidecadal and centennial scales, whereas variability of the SPL chronology is constrained to annual to decadal scales (Fig. 2A). First-order autoregressive modelling removed all low-frequency information (Fig. 2A, B).

Despite several statistical adjustments (power transformation, detrending, pre-whitening, variance adjustment) to account for sample size and inter-series correlation changes, the SPL residual chronology contains changes in variance that might produce spurious periods with increased/reduced drought and pluvial events. The SPL residual chronology reveals periods of reduced variance from the 12th to 14th century, during the 18th and since the 20th century (Fig. 3A).

To address the role of insufficient correction for heteroscedasticity as a potential driver of shifts in variance, we further examined the variance structure of 1000 residual chronologies with a constant yearly sample size of n = 80, and n = 15. The spread of the 100-year moving SD of these chronologies suggests that fluctuations in variance are persistent back in time and sample-size independent (Fig. 3B). In the second experiment, cambial age-alignment of the residual series, the corresponding 100-year moving SD patterns demonstrate that despite spread-level adjustments, variance in the residual dataset is still a function of tree age (Fig. 3C). Phases of high variability correspond to biologically younger states and phases of low variability correspond with older tree ages, which demonstrate that despite power transformation (Cook & Peters 1997), an age-dependent variance decline exists.

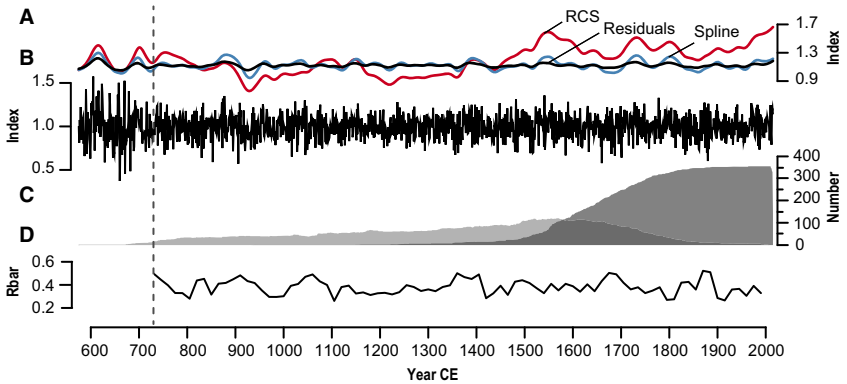

Fig. 2. Chronology characteristics. A. 50-year smoothed RCS (red), standard (blue) and SPL residual (black) chronologies. B. Uncorrected SPL residual chronology. C. Yearly sample size for relict and living material. D. Rbar statistics for the standard chronology (calculated over 30 years lagged by 15 years). The vertical dashed line indicates 730 CE when the EPS passes the 0.85 threshold.

As the dataset includes many old and slow-growing living trees with several individuals of nearly millennial age, and age heterogeneous relict material, due to different stages of weathering, tree age increases towards the present (Fig. 3D). With regard to age-effects in variance, age-class chronologies with homogenous age structures through the last millennium were created (Fig. 3D). Considering only age-segments of 1–200 and 201–400 years, a comparison of moving window SD patterns of the original SPL residual chronology with age-class residual chronologies demonstrates that shifts in variance are partially a function of the age structure of the dataset (Fig. 3E). For the entire dataset, in the 19th to 21st century, variance declines when tree age constantly increases and biologically old segments dominate. The age-structure adjustment relying solely on age segments between 1–200 or the ones between 201–400 demonstrates that for the post-1800 CE period, a homogenous age structure increases variance (Fig. 3E). To correct for this non-climatic artefact in variance, we used the arithmetic mean of the 1–200 and 201–400 SPL residual age-class chronologies for calibration and reconstruction (Fig. 3F). Despite these variance adjustments, additional decadal–centennial variance changes remain in the chronology that may represent changes in long-term precipitation variability (Fig. 3E).

TRW climate signals

Correlation work on PIHE TRW revealed growth–climate relationships are not stable in the low-frequency domain (Seim *et al.* 2012; Klippel *et al.* 2017). Calibration tests support these findings as no significant relationships ($p < 0.01$) between temperature, precipitation, SPI and the RCS and SPL standard chronologies are identified

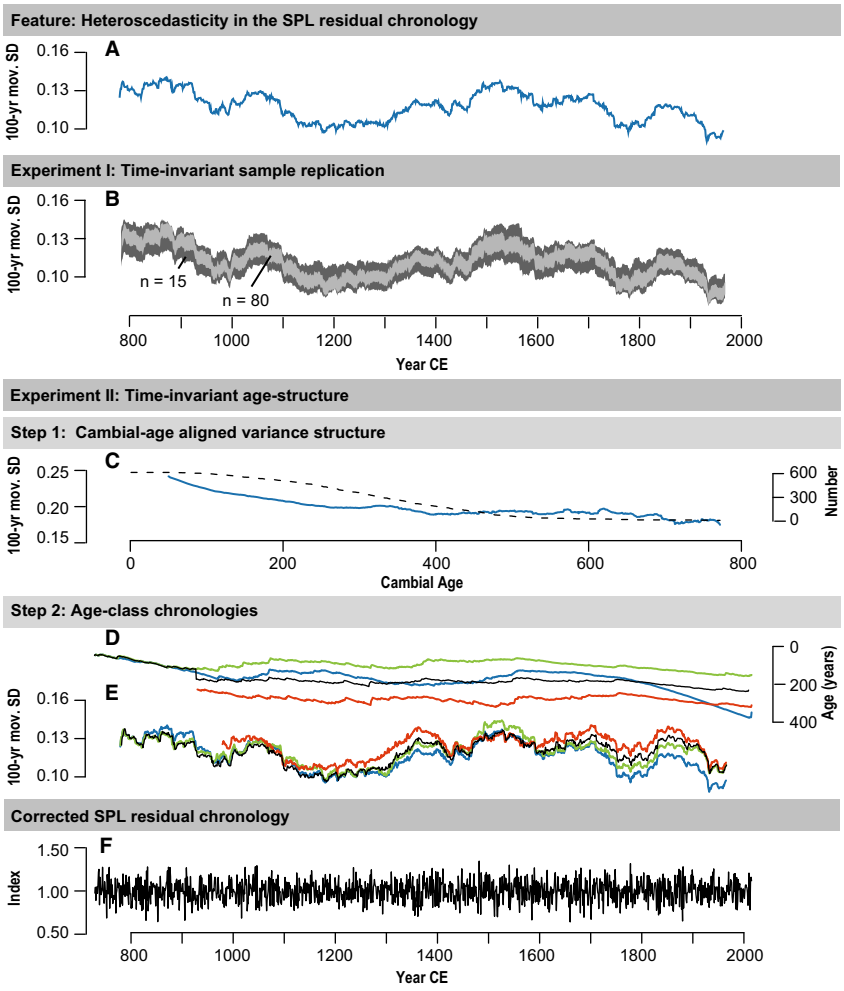

Fig. 3. Development of a variance-balanced chronology and analysis of sample size and tree age as potential biases. A. Heteroscedastic variance in the SPL residual chronology displayed as 100-year moving SD. B. Bandwidth of 100-year moving SD of 1000 artificially generated residual SPL chronologies (see Fig. S2) with constant yearly sample sizes of 80 (light grey) and 15 series (dark grey). C. 100-year moving SD of the mean of 615 cambial age-aligned individual residual series (blue) and sample replication (dashed line). D. Calendar year-aligned mean tree ages of the initial SPL residual chronology (blue), the SPL residual age-class chronologies 1–200 (green), 201–400 (red) and their average (black). E. Corresponding 100-year moving SD. F. The age structure-corrected SPL residual chronology used for calibration and reconstruction.

(Fig. S2). Correlation analysis of the SPL residual chronology with SPI and precipitation data shows that the high-frequency TRW variations mirror moisture changes, with the highest coefficients being achieved using SPI as a calibration target. Therefore, we focused on high-frequency hydro-climatic changes, calibrating the SPL residual chronology against 1-month and 2-month SPI. However, using only data from the closest grid (20.5–21°E/40–40.5°N) over the common 1961–2015 proxy-target period (r = 0.43), the correlation with SPI is neither high nor temporally stable (Figs 4A, S3). However, a spatial analysis relying on gridded data reveals a robust correlation pattern with 2-month SPI in June–July with Pearson correlations ranging from 0.43 to 0.66. A strong correlation is found north of the study region with grids over the central part of the Balkan Peninsula between 40–45° N and 20–25° E, including Albania, Bulgaria, Greece, Kosovo, Macedonia, Romania and Serbia (Fig. 4B). With the exception of some correlations with grid-cells over the mountainous mainland of Greece, SPI data covering the peninsular coast have no significant influence (Fig. 4B). Average SPIs for all grids that show a significant correlation with the SPL residual chronology at $p < 0.001$ return a $r_{1961–2015} = 0.68$ correlation in June–July (Fig. 4C).

Calibration/verification tests

The SPL residual chronology explains 48% of the 2-month $SPI_{June–July}$ variance over the 1988–2015 calibration period (Fig. 5A). RE and CE scores of the corresponding 1961–1988 verification period are 0.42 each, and DW-statistics indicate no autocorrelation in the model residuals. Transposing the periods and using 1961–1988 for calibration, the SPL residual chronology explains 47% of SPI variance, RE and CE scores of the corresponding 1988–2015 verification period are 0.46 and 0.45, respectively, and DW-statistics indicate no autocorrelation (Fig. 5B). Calibration/verification procedures indicate a stable relationship; therefore, we used the entire 1961–2015 period to develop a linear model for the reconstruction:

$$\text{2-month SPI}_{\text{June–July}} = 4.7 + (-4.7 \times {}_{\text{residual}}\,\text{SPL}) \quad (1)$$

Identification of extreme years and variance changes

In total, the reconstruction contains 51 dry and 43 pluvial events exceeding the ±1 SD threshold since 730 CE (Fig. 6). We identified a total of 72 new extreme events, 59 of which date prior to the 17th century. The driest and wettest years in the reconstruction are 1660 CE (−1.7 SD) and 1482 (+1.6 SD). The highest numbers of extremes were reconstructed during the 9th and 19th centuries, whereas the 12th century was characterized by few extremes. Extremes within the calibration period were the dry events of 1987 and 2012, and the pluvial event of 1970. Extreme dry and wet events of 2-year duration occurred in 1517–1518, 1861–1862 and 737–738. Seemingly, extreme dry and pluvial events appear in decadal clusters, e.g. 822, 824, 830, 831, 833 and 1045, 1052, 1044, 1047 and 1880, 1873 and 1881, whereas we also find multiple decades without extreme events.

Discussion

We present the first PIHE-based reconstruction of hydro-climatic conditions for the Balkan Peninsula in the eastern Mediterranean from 730–2015 CE. The reconstruction is

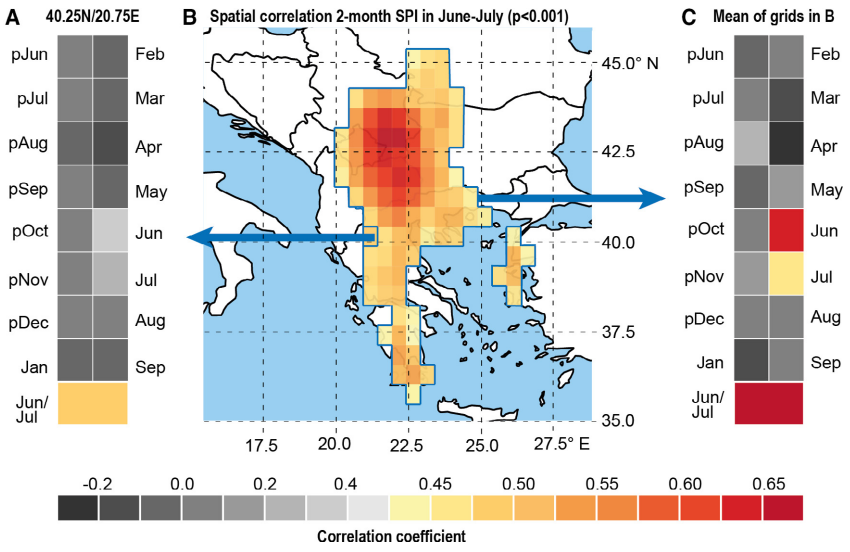

Fig. 4. Chronology calibration. A. SPL residual chronology correlated over the 1961–2015 period with 1-month SPI and 2-month SPI June–July based on precipitation data from the 0.5° grid 40.25°N/20.75°E. B. Spatial extent of significant ($p \leq 0.001$) correlations of the SPL residual chronology and the 0.5° 2-month SPI June–July. C. Same as (A) but the 1-month SPI and 2-month SPI June–July are averages of all grids displayed in (B).

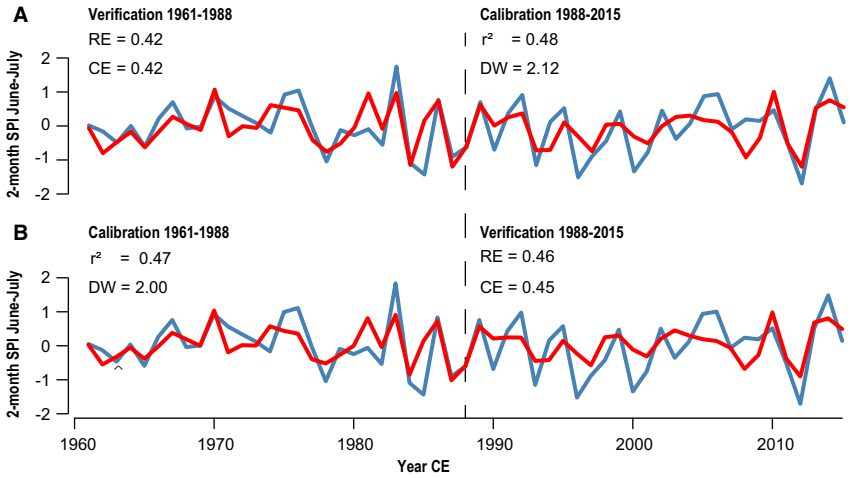

Fig. 5. Calibration and verification statistics for the grid-based 2-month SPI June–July reconstruction; blue lines indicate actual 2-month SPI June–July values and red lines the tree-ring derived estimates.

based on a compilation of 615 TRW measurements reaching back to 575 CE. The record's length makes it currently the longest PIHE TRW chronology.

Chronology characteristics and heteroscedasticity

The application of different standardization approaches demonstrates that PIHE TRW contains high-, medium- and low-frequency variance. RCS allows climatic information to be preserved on time scales longer than the individual segments and long-term changes in environmental conditions are also preserved (Cook *et al.* 1995). When applying RCS to this dataset, one needs to be aware of the contemporaneous old slow-growing trees as well as the relict material of mixed biological ages due to weathering. The significance of this combination on the low-frequency signal is not fully understood (Esper *et al.* 2003). However, RCS is used to evaluate potential low-frequency signals and to estimate the potential loss of low-frequency variance in the SPL residual chronology (Cook *et al.* 1995).

Our analysis has shown that despite the application of standardization procedures we still find a systematic relationship between tree age and chronology variance, even after removing much of the low-frequency variability in the SPL residual chronology (Carrer & Urbinati 2004; Esper *et al.* 2008; Linares *et al.* 2013; Konter *et al.* 2016). When using old slow-growing living trees only, mean segment length and tree age increase over time, resulting in a constant decrease in variance. We homogenized these age changes by creating two age-class chronologies that cover 1–200 years and 201–400 years, respectively, and by using the arithmetic mean chronology for reconstruction. This assessment underscored the importance of heterogeneous tree ages for the calculation of unbiased tree-ring chronologies, as systematic tree-age changes add noise to the variance structure of a chronology (Frank *et al.* 2007a; Büntgen *et al.* 2015). These changes might affect the climate sensitivity of tree growth (Yu *et al.* 2008; Linares *et al.* 2013) and impact the magnitude and frequency of extreme events.

Hydro-climatic signal

The application of different detrending and filter techniques shows that the chronology mirrors high-frequency hydro-climatic changes more closely than low-

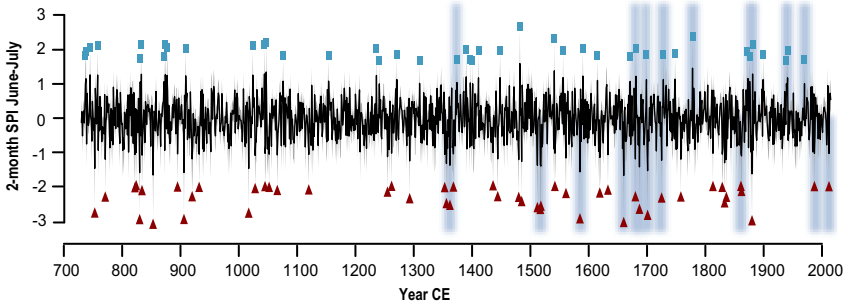

Fig. 6. 2-month SPI June–July reconstruction (black) and calibration uncertainty estimates (grey) since 730 CE. Blue and red symbols indicate extreme events exceeding ±1 SD. Symbols are added at the tips of the uncertainty range. Shading indicates extreme events verified by historical documents or previous hydro-climate reconstructions.

frequency changes. Potential reasons for this discrepancy in the low-frequency domain include (i) a nonlinearity or decoupling of the growth/climate response on longer time scales (Fritts 1976); (ii) the more white precipitation spectrum compared to the red temperature spectrum (Ault & St. George 2010); (iii) potential biases in long-term trends inherent to instrumental data, e.g. caused by station relocations or changes in their operating system (Dienst *et al.* 2017); and (iv) the difficulty in preserving low-frequency variance in TRW (Esper *et al.* 2002). As also the reliable instrumental target extends only over 55 years back to 1961, the full spectrum of potential SPI variability, and particularly the low-frequency end of that spectrum over longer time scales remains unaddressed.

In the high-frequency domain, tree growth is positively affected by moist summer conditions. This association is manifested by the high correlation between TRW and the 2-month SPI from June–July ($r > 0.43$, $p < 0.001$). We assume that cell production including enlargement in June–July is associated with stomatal responses to water availability that control water losses (Vieira *et al.* 2013). To avoid drought-induced hydraulic failure, stomata closure maintains a water potential above the threshold of xylem cavitation (Loustau *et al.* 1996) and metabolic processes like cell formation break down (Cherubini *et al.* 2003; McDowell *et al.* 2008; Hartl-Meier *et al.* 2015).

Spatial analysis reveals that the core region with highest 2-month SPI correlation from June–July ($r = 0.68$, $p < 0.001$) extends to a distance of 320 km from the study site, and that grids covering the Pindus range and coast have minor or no significance. This is possibly due to the great spatial variability of precipitation caused by regional synoptic patterns and the orographic settings (Bolle 2003). During June and July, cool and dry Etesian winds blow from the Aegean Basin (Metaxas & Bartzokas 1994). These Etesian winds arise in conjunction with a low-pressure system located over the eastern Mediterranean and Near East, and a high-pressure system over the Balkan Peninsula (Repapis *et al.* 1978; Tritakis 1984). The frequency and force of these winds depend upon the strength of the pressure systems (Metaxas & Bartzokas 1994). We assume that the strength of the high-pressure cell situated over the central Balkan Peninsula modulates precipitation over the Pindus Mountains, commonly in the form of thunderstorms (Marinaki *et al.* 2006). We assume a more pronounced warming and enhanced atmospheric instability in this region due to an increased continental climate, favouring the emergence of thunderstorms, which penetrate into the Pindus Mountains from the north. Additionally, the remoteness of meteorological stations and the weighting of the data used for interpolation of the grid cells affect the spatial patterns. Grid cells differ by station data and weighting (Harris *et al.* 2014), causing differences in climate signal strength.

Drought history

We developed a 1286-year-long SPI reconstruction representative of a large area of the Balkan Peninsula (Fig. 6). As proxy data from the region are limited, we substantially improved our understanding of annually resolved hydroclimate prior to the LIA by producing a millennium length reconstruction. For the first time, regional evidence of past drought and pluvial events is extended back to 730 CE. Multiple drought events, 59 (32) prior to the 17th (11th) century were detected, notably the exceptional 1482 pluvial.

TRW explains about 47% of the regional 2-month SPI June–July variance from 1961 to 2015. The explained variance lies within the range of previous SPI reconstructions developed in Romania (45%), Spain (40%), Sweden (45%, Seftigen *et al.* 2013) and Turkey (43%, Touchan *et al.* 2005). To assess patterns of past European precipitation variability, the new SPI estimates were compared with existing reconstructions from Spain (1694–2012, Tejedor *et al.* 2016) and Romania (1688–2010, Levanic *et al.* 2012) (in Fig. S4A, only Levanic *et al.*'s data are displayed). Whereas no significant correlation with the more remote reconstruction from Spain is found ($r_{1694–2012} = 0.002$), the Romanian and our reconstructions correlate at $r_{1758–2015} = 0.31$ (Fig. S4B), suggesting a spatial coherence in drought variability over the Balkan Peninsula, probably driven by synoptic scale circulation (Xoplaki *et al.* 2003, 2004). 31-year moving correlations between the Romanian and our record reveal an amplified coherency over time with increasing sample size in the Romanian record, and stable associations when EPS exceeds 0.85 (Fig. S2C; Wigley *et al.* 1984).

Our reconstruction fills a spatial gap in a network of hydro-climatic records over the Balkan Peninsula and the eastern Mediterranean and refines our understanding of the spatial extent of hydro-climatic extremes. By comparing all regional hydro-climatic reconstructions (e.g. drought, sunshine, precipitation) and historical records from Turkey (Purgstall 1983) and Spain (Alberola 1996) for the period of data overlap, we find a general correspondence between the strength of an event in our reconstruction and a number of historical/proxy pieces of evidence. The events in 1660 CE and 1725 CE are examples of severe droughts that extend over the entire Mediterranean. Over the Balkan Peninsula and eastern Mediterranean, the extremely dry summer of 1660 is captured in all tree-ring based climate reconstructions (D'Arrigo & Cullen 2001; Akkemik & Aras 2005; Akkemik *et al.* 2005, 2008; Touchan *et al.* 2005; Griggs *et al.* 2007; Köse *et al.* 2011), a finding that is consistent with historical documents reporting catastrophic fires and famines in Anatolia (Purgstall 1983). The dry summer of 1725 appears in drought reconstructions from Bosnia and Herzegovina, Greece, Romania, Spain and Turkey (Akkemik & Aras 2005; Akkemik *et al.* 2005; Köse *et al.* 2011; Levanic *et al.* 2012; Poljanšek *et al.*

2013; Klesse *et al.* 2015; Tejedor *et al.* 2016), and is verified in historical documents from Spain reporting a year without harvest (Alberola 1996).

The drought event in 1987 CE was spatially restricted to the Balkan Peninsula and does not appear in reconstructions from Turkey. The 1987 dry summer appeared as a narrow/negative pointer year in a PIHE chronology from Bulgaria when nearby climate stations recorded very dry conditions in June (Panayotov *et al.* 2010). In the same year, dry summer conditions were recorded in Romania (Levanic *et al.* 2012) and extremely dry June–August conditions were measured in Slovakia (Büntgen *et al.* 2009).

Extremes with regional-scale influence include pluvial events in 1881 CE and 1970 CE. The 1881 event is described as outstanding in Turkey (Akkemik *et al.* 2005, 2008; Köse *et al.* 2011) and Romania (Levanic *et al.* 2012). The wet summer of 1970 appears in multiple hydro-climatic reconstructions from Romania, Slovakia and Turkey (Akkemik *et al.* 2008; Büntgen *et al.* 2009; Levanic *et al.* 2012) and is also mentioned as a positive pointer year in Bulgaria (Panayotov *et al.* 2010).

Although characterized by high proxy data availability, multiple extreme events in the post-17th century period e.g. 1633, 1748, 1829, 1873 and 1899 CE, could not be linked with previous reconstructions or documentary evidence. As these extremes only slightly pass the threshold of ±1 SD, we assume they were caused by local environmental conditions.

Remaining uncertainties

We note that periods with extreme events in the reconstruction correspond to periods with high variance and periods without extreme events to periods with low variance. Despite statistical and age-structure adjustments (described above), the final reconstruction reveals periods of increased drought and pluvial events and a decadal clustering of several extremes (Fig. 6). The mechanisms of these long-term changes in extreme event occurrence remain unclear. We interpret phases with a lower/higher variance as stages of more balanced/variable climatic conditions, and assume no time-dependent biases due to variance fluctuations that obscure the frequency of extreme events on decadal scales (Frank *et al.* 2007b). Over Spain, a linkage between summer warming and an increased frequency of extreme drought events during the 20th and 21st century has been identified (Tejedor *et al.* 2016). However, at the high-elevation sites of Mt Smolikas, the current aridification over the Mediterranean (Maheras & Anagnostopoulou 2003; García-Herrera *et al.* 2007) does not impair tree growth as PIHE does not show any increased drought sensitivity in our study. We suggest that the current warming has increased the regional strength of orographic rainfall (Evans 2009; Black *et al.* 2010) and that PIHE now benefits from the addition, although these assumptions require further testing.

Methodological considerations are unique to every proxy-climate reconstruction experiment, limiting inter-study comparisons of the frequency and magnitude of extremes. Ecological settings are heterogeneous, e.g. high elevation vs. low elevation (Griggs *et al.* 2007), and target parameters differ, e.g. SPI vs. precipitation (Klesse *et al.* 2015). In addition, extreme events are frequently defined differently: e.g. events that exceed ±1 SD (Touchan *et al.* 2005; Köse *et al.* 2011), ±1.76 SD (Türkes 1996; Akkemik & Aras 2005; Tejedor *et al.* 2016) and events that are ±2 SD (Köse *et al.* 2011) above or below the mean. These thresholds often correspond to percentiles of the observed data for the calibration period (Touchan *et al.* 2008) or are based on a fixed amount of extreme events, e.g. the 20 most positive/negative reconstructed values (Büntgen *et al.* 2009).

Conclusions

Based on a network of high-elevation sites on Mt Smolikas in the Pindus Mountains, Greece, regional summer drought variability was reconstructed for the first time back to 730 CE. Summer drought was most severe in 1660 and climatic conditions most pluvial in 1482. Our reconstruction provides new insight on hydro-climatic variability in the northeastern Mediterranean, especially prior to the LIA, and fills a temporal and spatial gap in a larger scale drought reconstruction network (Griggs *et al.* 2007; Akkemik *et al.* 2008; Büntgen *et al.* 2009; Köse *et al.* 2011). We find that the frequency of extreme events has been variable, especially in the 20th century when the number of droughts considerably reduced. A set of tests, including power transformation (Cook & Peters 1997), variance stabilization (Frank *et al.* 2007b), pre-whitening, correction for age biases (Carrer & Urbinati 2004; Esper *et al.* 2008; Linares *et al.* 2013; Konter *et al.* 2016), and homogenizing tree age over time, showed that the variance change in the 20th century is not related to replication or inter-series correlation. We have successfully extended information on past hydro-climate variability into the first millennium and conclude that knowledge of the hydro-climatological history of the region has been markedly improved, especially prior to the LIA.

Acknowledgements. – This study was supported by the German Research Foundation (DFG, ES 161/9-1) and National Science Foundation CAREER grant (NSF-CAREER #1349942). We thank Tilmann Büttner, Markus Kochbeck, Oliver Konter, Amarita Krusic, Anna Krusic, Jonas Krusic, Fredrik C. Ljungqvist, Matthew Meko, Valerie Trouet and Sam Williams for valuable assistance in the field; Tom Levanič and Ernesto Tejedor for providing SPI reconstructions; and two reviewers for helpful suggestions. The authors declare no conflict of interest.

References

Akkemik, U. & Aras, A. 2005: Reconstruction (1689–1994 AD) of April–August precipitation in the southern part of central Turkey. *International Journal of Climatology 25*, 537–548.

Akkemik, U., Dagdeviren, N. & Aras, A. 2005: A preliminary reconstruction (A.D. 1635–2000) of spring precipitation using oak tree rings

in the western Black Sea region of Turkey. *International Journal of Biometeorology 49*, 297–302.

Akkemik, U., D'Arrigo, R., Cherubini, P., Kose, N. & Jacoby, G. C. 2008: Tree-ring reconstructions of precipitation and streamflow for north-western Turkey. *International Journal of Climatology 28*, 173–183.

Alberola, A. 1996: La percepción de la catástrofe: sequía e inundaciones en tierras valencianas durante la primera mitad del siglo XVIII. *Revista de Historia Moderna 15*, 257–299.

Ault, T. R. & St. George, S. 2010: The magnitude of decadal and multidecadal variability in North American precipitation. *Journal of Climate 23*, 842–850.

Black, E., Brayshaw, D. J. & Rambeau, C. M. 2010: Past, present and future precipitation in the Middle East: insights from models and observations. *Philosophical Transactions of the Royal Society A, Mathematical, Physical and Engineering Sciences 368*, 5173–5184.

Bolle, H.-J. 2003: *Mediterranean Climate*. 371 pp. Springer, Berlin.

Bräker, O. U. 1981: Der Alterstrend bei Jahrringdichten und Jahrringbreiten von Nadelhölzern und sein Ausgleich. *Mitteilungen der Forstlichen Bundes-Versuchsanstalt Wien 142*, 75–102.

Brandes, R. 2007: *Waldgrenzen griechischer Hochgebirge: Unter besonderer Berücksichtigung des Taygetos, Südpeloponnes*. 296 pp. Friedrich-Alexander-Universität Erlangen-Nürnberg, Erlangen.

Briffa, K. R., Jones, P. D., Bartholin, T. S., Eckstein, D., Schweingruber, F. H., Karlen, W., Zetterberg, P. & Eronen, M. 1992: Fennoscandian summers from AD-500 - temperature-changes on short and long timescales. *Climate Dynamics 7*, 111–119.

Briffa, K. R., Jones, P. D., Pilcher, J. R. & Hughes, M. K. 1988: Reconstructing summer temperatures in northern Fennoscandinavia back to A.D. 1700 using tree-ring data from Scots pine. *Arctic and Alpine Research 20*, 385–394.

Büntgen, U., Brázdil, R., Frank, D. & Esper, J. 2009: Three centuries of Slovakian drought dynamics. *Climate Dynamics 35*, 315–329.

Büntgen, U., Trnka, M., Krusic, P. J., Kyncl, T., Kyncl, J., Luterbacher, J., Zorita, E., Ljungqvist, F. C., Auer, I., Konter, O., Schneider, L., Tegel, W., Štěpánek, P., Brönnimann, S., Hellmann, L., Nievergelt, D. & Esper, J. 2015: Tree-ring amplification of the early nineteenth-century summer cooling in Central Europe. *Journal of Climate 28*, 5272–5288.

Carrer, M. & Urbinati, C. 2004: Age-dependent tree-ring growth responses to climate in *Larix decidua* and *Pinus cembra*. *Ecology 85*, 730–740.

Cherubini, P., Gartner, B. L., Tognetti, R., Bräker, O. U., Schoch, W. & Innes, J. L. 2003: Identification, measurement and interpretation of tree rings in woody species from Mediterranean climates. *Biological Reviews of the Cambridge Philosophical Society 78*, 119–148.

Cook, E. R. 1985: *A time series analysis approach to tree ring standardization*. Ph.D. thesis, University of Arizona, Tucson, 37 pp.

Cook, E. R. & Peters, K. 1997: Calculating unbiased tree-ring indices for the study of climatic and environmental change. *Holocene 7*, 361–370.

Cook, E. R., Briffa, K. R. & Jones, P. D. 1994: Spatial regression methods in dendroclimatology: a review and comparison of two techniques. *International Journal of Climatology 14*, 379–402.

Cook, E., Briffa, K. R., Meko, D. M., Graybill, D. & Funkhouser, G. 1995: The 'segment length curse' in long tree-ring chronology development for palaeoclimatic studies. *The Holocene 5*, 229–237.

Cook, E., Krusic, P. J., Peters, K. & Holmes, R. L. 2017: *Program ARSTAN; version 48d2, Autoregressive tree-ring standardization program*. Available at: http://www.ldeo.columbia.edu/tree-ring-laboratory/resources/software.

Cufar, K., De Luis, M., Eckstein, D. & Kajfez-Bogataj, L. 2008: Reconstructing dry and wet summers in SE Slovenia from oak tree-ring series. *International Journal of Biometeorology 52*, 607–615.

D'Arrigo, R. & Cullen, H. M. 2001: A 350-year (AD 1628–1980) reconstruction of Turkish precipitation. *Dendrochronologia 19*, 169–177.

Dienst, M., Linden, J., Engstrom, E. & Esper, J. 2017: Removing the relocation bias from the 155-year Haparanda temperature record in Northern Europe. *International Journal of Climatology 37*, 4015–4026.

Diffenbaugh, N. S. & Giorgi, F. 2012: Climate change hotspots in the CMIP5 global climate model ensemble. *Climatic Change 114*, 813–822.

Dubrovský, M., Hayes, M., Duce, P., Trnka, M., Svoboda, M. & Zara, P. 2013: Multi-GCM projections of future drought and climate variability indicators for the Mediterranean region. *Regional Environmental Change 14*, 1907–1919.

Durbin, J. & Watson, G. S. 1951: Testing for serial correlation in least squares regression. *Biometrika 38*, 159–178.

Esper, J., Cook, E. R., Krusic, P. J., Peters, K. & Schweingruber, F. H. 2003: Tests of the RCS method for preserving low-frequency variability in long tree-ring chronologies. *Tree-Ring Research 59*, 81–98.

Esper, J., Cook, E. R. & Schweingruber, F. H. 2002: Low-frequency signals in long tree-ring chronologies for reconstructing past temperature variability. *Science 295*, 2250–2253.

Esper, J., Frank, D., Büntgen, U., Verstege, A. & Luterbacher, J. 2007: Long-term drought severity variations in Morocco. *Geophysical Research Letters 34*, L17702, https://doi.org/10.1029/2007gl030844.

Esper, J., Frank, D. C., Wilson, R. J. S. & Briffa, K. R. 2005: Effect of scaling and regression on reconstructed temperature amplitude for the past millennium. *Geophysical Research Letters 32*, L07711, https://doi.org/10.1029/2004gl021236.

Esper, J., Krusic, P. J., Ljungqvist, F. C., Luterbacher, J., Carrer, M., Cook, E., Davi, N. K., Hartl-Meier, C., Kirdyanov, A., Konter, O., Myglan, V., Timonen, M., Treydte, K., Trouet, V., Villalba, R., Yang, B. & Büntgen, U. 2016: Ranking of tree-ring based temperature reconstructions of the past millennium. *Quaternary Science Reviews 145*, 134–151.

Esper, J., Niederer, R., Bebi, P. & Frank, D. 2008: Climate signal age effects—Evidence from young and old trees in the Swiss Engadin. *Forest Ecology and Management 255*, 3783–3789.

Evans, J. P. 2009: Global warming impact on the dominant precipitation processes in the Middle East. *Theoretical and Applied Climatology 99*, 389–402.

Fischer, E. M. & Schar, C. 2010: Consistent geographical patterns of changes in high-impact European heatwaves. *Nature Geoscience 3*, 398–403.

Fotiadi, A. K., Metaxas, D. A. & Bartzokas, A. 1999: A statistical study of precipitation in northwest Greece. *International Journal of Climatology 19*, 1221–1232.

Frank, D., Büntgen, U., Böhm, R., Maugeri, M. & Esper, J. 2007a: Warmer early instrumental measurements versus colder reconstructed temperatures: shooting at a moving target. *Quaternary Science Reviews 26*, 3298–3310.

Frank, D., Esper, J. & Cook, E. R. 2007b: Adjustment for proxy number and coherence in a large-scale temperature reconstruction. *Geophysical Research Letters 34*, L16709, https://doi.org/10.1029/2007gl030571.

Fritts, H. C. 1976: *Tree Rings and Climate*. 567 pp. Blackburn Press, Caldwell.

Gao, X. J. & Giorgi, F. 2008: Increased aridity in the Mediterranean region under greenhouse gas forcing estimated from high resolution simulations with a regional climate model. *Global and Planetary Change 62*, 195–209.

García-Herrera, R., Hernández, E., Barriopedro, D., Paredes, D., Trigo, R. M., Trigo, I. F. & Mendes, M. A. 2007: The outstanding 2004/05 drought in the Iberian Peninsula: associated atmospheric circulation. *Journal of Hydrometeorology 8*, 483–498.

Giorgi, F. & Lionello, P. 2008: Climate change projections for the Mediterranean region. *Global and Planetary Change 63*, 90–104.

Griggs, C., DeGaetano, A., Kuniholm, P. & Newton, M. 2007: A regional high-frequency reconstruction of May–June precipitation in the north Aegean from oak tree rings, A.D. 1089–1989. *International Journal of Climatology 27*, 1075–1089.

Harris, I., Jones, P. D., Osborn, T. J. & Lister, D. H. 2014: Updated high-resolution grids of monthly climatic observations - the CRU TS3.10 Dataset. *International Journal of Climatology 34*, 623–642.

Hartl-Meier, C., Zang, C., Büntgen, U., Esper, J., Rothe, A., Gottlein, A., Dirnbock, T. & Treydte, K. 2015: Uniform climate sensitivity in tree-ring stable isotopes across species and sites in a mid-latitude temperate forest. *Tree Physiology 35*, 4–15.

Holmes, R. L. 1983: Computer-assisted quality control in tree-ring dating and measurement. *Tree-Ring Bulletin 43*, 69–78.

Klesse, S., Ziehmer, M., Rousakis, G., Trouet, V. & Frank, D. 2015: Synoptic drivers of 400 years of summer temperature and precipitation variability on Mt. Olympus, Greece. *Climate Dynamics 45*, 807–824.

Klippel, L., Krusic, P. J., Brandes, R., Hartl-Meier, C., Trouet, V., Meko, M. & Esper, J. 2017: High-elevation inter-site differences in Mount Smolikas tree-ring width data. *Dendrochronologia 44*, 164–173.

Konter, O., Büntgen, U., Carrer, M., Timonen, M. & Esper, J. 2016: Climate signal age effects in boreal tree-rings: lessons to be learned for paleoclimatic reconstructions. *Quaternary Science Reviews 142*, 164–172.

Konter, O., Krusic, P. J., Trouet, V. & Esper, J. 2017: Meet Adonis, Europe's oldest dendrochronologically dated tree. *Dendrochronologia 42*, p.12.

Köse, N., Akkemik, Ü., Dalfes, H. N. & Özeren, M. S. 2011: Tree-ring reconstructions of May–June precipitation for western Anatolia. *Quaternary Research 75*, 438–450.

Lange, W., Janezic, T. S. & Spanoudaki, M. 1994: Cembratrienols and other components of white-bark pine (*Pinus heldreichii*) Oleoresin. *Phytochemistry 36*, 1277–1279.

Levanic, T., Popa, I., Poljansek, S. & Nechita, C. 2012: A 323-year long reconstruction of drought for SW Romania based on black pine (*Pinus Nigra*) tree-ring widths. *International Journal of Biometeorology 57*, 703–714.

Linares, J. C., Taïqui, L., Sangüesa-Barreda, G., Seco, J. I. & Camarero, J. J. 2013: Age-related drought sensitivity of Atlas cedar (*Cedrus atlantica*) in the Moroccan Middle Atlas forests. *Dendrochronologia 31*, 88–96.

Ljungqvist, F. C., Krusic, P. J., Sundqvist, H. S., Zorita, E., Brattstrom, G. & Frank, D. 2016: Northern Hemisphere hydroclimate variability over the past twelve centuries. *Nature 532*, 94–98.

Loukas, A., Vasiliades, L. & Dalezios, N. R. 2002: Hydroclimatic variability of regional droughts in Greece using the palmer moisture anomaly index. *Nordic Hydrology 33*, 425–442.

Loustau, D., Breda, N. & Granier, A. 1996: Transpiration of a 64-year-old maritime pine stand in Portugal. 1. Seasonal course of water flux through maritime pine. *Oecologia 107*, 33–42.

Maheras, P. & Anagnostopoulou, C. 2003: Circulation types and their Influence on the interannual variability and precipitation changes in Greece. *In* Bolle, H.-J. (ed.): *Mediterranean Climate*, 215–239. Springer, Berlin.

Marinaki, A., Spiliotopoulos, M. & Michalopoulou, H. 2006: Evaluation of atmospheric instability indices in Greece. *Advances in Geosciences 7*, 131–135.

McDowell, N., Pockman, W. T., Allen, C. D., Breshears, D. D., Cobb, N., Kolb, T., Plaut, J., Sperry, J., West, A., Williams, D. G. & Yepez, E. A. 2008: Mechanisms of plant survival and mortality during drought: why do some plants survive while others succumb to drought? *New Phytologist 178*, 719–739.

McKee, T. B., Doesken, N. J. & Kleist, J. 1993: The relationship of drought frequency and duration to time scales. *Eighth Conference on Applied Climatology*. 179–184 pp. Colorado State University, Anaheim.

Metaxas, D. A. & Bartzokas, A. 1994: Pressure covariability over the Atlantic, Europe and N Africa - application - centers of Action for temperature, winter precipitation and summer winds in Athens, Greece. *Theoretical and Applied Climatology 49*, 9–18.

Nastos, P. T. & Kapsomenakis, J. 2015: Regional climate model simulations of extreme air temperature in Greece. Abnormal or common records in the future climate? *Atmospheric Research 152*, 43–60.

Panayotov, M., Bebi, P., Trouet, V. & Yurukov, S. 2010: Climate signal in tree-ring chronologies of *Pinus peuce* and *Pinus heldreichii* from the Pirin Mountains in Bulgaria. *Trees-Structure and Function 24*, 479–490.

Pasho, E., Camarero, J. J., de Luis, M. & Vicente-Serrano, S. M. 2011: Impacts of drought at different time scales on forest growth across a wide climatic gradient in north-eastern Spain. *Agricultural and Forest Meteorology 151*, 1800–1811.

Poljanšek, S., Ceglar, A. & Levanič, T. 2013: Long-term summer sunshine/moisture stress reconstruction from tree-ring widths from Bosnia and Herzegovina. *Climate of the Past 9*, 27–40.

Purgstall, B. 1983: *Ottoman State History. Volumes 1–7*. Üçdal Publishing, Istanbul.

R Core Team 2017: *R A language and environment for statistical computing*. R Foundation for Statistical Computing, Vienna, Austria. Available at: https://www.r-project.org/. (accessed 16.01.2018).

Repapis, C., Zerefos, C. & Tritakis, B. 1978: On the Etesians over the Aegean. *Proceedings of the Academy of Athens 52*, 572–606.

Rinn, F. 2003: *Time Series Analysis and Presentation for Dendrochronology and Related Applications*. Available at: http://www.rimatech.com.

Schneider, L., Smerdon, J. E., Büntgen, U., Wilson, R. J. S., Myglan, V. S., Kirdyanov, A. V. & Esper, J. 2015: Revising midlatitude summer temperatures back to A.D. 600 based on a wood density network. *Geophysical Research Letters 42*, 4556–4562.

Seftigen, K., Linderholm, H. W., Drobyshev, I. & Niklasson, M. 2013: Reconstructed drought variability in southeastern Sweden since the 1650s. *International Journal of Climatology 33*, 2449–2458.

Seim, A., Büntgen, U., Fonti, P., Haska, H., Herzig, F., Tegel, W., Trouet, V. & Treydte, K. 2012: Climate sensitivity of a millennium-long pine chronology from Albania. *Climate Research 51*, 217–228.

Tejedor, E., de Luis, M., Cuadrat, J. M., Esper, J. & Saz, M. A. 2016: Tree-ring-based drought reconstruction in the Iberian Range (east of Spain) since 1694. *International Journal of Biometeorology 60*, 361–372.

Todaro, L., Andreu, L., D'Alessandro, C. M., Gutirrez, E., Cherubinic, P. & Saracino, A. 2007: Response of *Pinus leucodermis* to climate and anthropogenic activity in the National Park of Pollino (Basilicata, Southern Italy). *Biological Conservation 137*, 507–519.

Touchan, R., Funkhouser, G., Hughes, M. K. & Erkan, N. 2005: Standardized precipitation index reconstructed from Turkish tree-ring widths. *Climatic Change 72*, 339–353.

Touchan, R., Meko, D. M. & Aloui, A. 2008: Precipitation reconstruction for Northwestern Tunisia from tree rings. *Journal of Arid Environments 72*, 1887–1896.

Tritakis, V. P. 1984: Possible solar signature on a well-established weather phenomenon. *Journal of Geophysical Research-Atmospheres 89*, 2609–2615.

Trouet, V., Panayotov, M. P., Ivanova, A. & Frank, D. 2012: A pan-European summer teleconnection mode recorded by a new temperature reconstruction from the northeastern Mediterranean (AD 1768–2008). *Holocene 22*, 887–898.

Türkes, M. 1996: Meteorological drought in Turkey: a historical perspective, 1930–93. *Drought Network News 8*, 17–21.

Vieira, J., Rossi, S., Campelo, F., Freitas, H. & Nabais, C. 2013: Seasonal and daily cycles of stem radial variation of *Pinus pinaster* in a drought-prone environment. *Agricultural and Forest Meteorology 180*, 173–181.

Wigley, T., Briffa, K. R. & Jones, P. D. 1984: On the average of correlated time series, with applications in dendroclimatology and hydrometeorology. *Journal of Climate and Applied Meteorology 23*, 201–2013.

Wilson, R., Anchukaitis, K., Briffa, K. R., Büntgen, U., Cook, E., D'Arrigo, R., Davi, N., Esper, J., Frank, D., Gunnarson, B., Hegerl, G., Helama, S., Klesse, S., Krusic, P. J., Linderholm, H. W., Myglan, V., Osborn, T. J., Rydval, M., Schneider, L., Schurer, A., Wiles, G., Zhang, P. & Zorita, E. 2016: Last millennium northern hemisphere summer temperatures from tree rings: part I: the long term context. *Quaternary Science Reviews 134*, 1–18.

Xoplaki, E., Gonzalez-Rouco, J. F., Gyalistras, D., Luterbacher, J., Rickli, R. & Wanner, H. 2003: Interannual summer air temperature variability over Greece and its connection to the large-scale atmospheric circulation and Mediterranean SSTs 1950–1999. *Climate Dynamics 20*, 537–554.

Xoplaki, E., Gonzalez-Rouco, J. F., Luterbacher, J. & Wanner, H. 2004: Wet season Mediterranean precipitation variability: influence of large-scale dynamics and trends. *Climate Dynamics 23*, 63–78.

Yu, G., Liu, Y., Wang, X. & Ma, K. 2008: Age-dependent tree-ring growth responses to climate in Qilian juniper (*Sabina przewalskii* Kom.). *Trees 22*, 197–204.

Supporting Information

Additional supplemental material may be found online in the Supporting Information section at the end of the article.

Fig. S1. Calendar year specific series decomposition and generation of homogenous time series. A. From 615 residual series. B. 1000 artificial residual series spanning the period 730–2015 CE were generated by a new random composition of calendar year specific values. C. 1000 mean chronologies, of which 80 (15) were randomly selected to create subset residual chronologies.

Fig. S2. Correlation coefficients of the SPL residual (red), SPL standard (yellow) and RCS (green) chronologies with 1-month and 2-month A. temperature, B. precipitation and C. SPI data derived from the 20.5–21°E/40–40.5°N grid cell for the period 1961–2015. Dashed lines indicate $p < 0.01$ threshold.

Fig. S3. 31-year moving window correlations between the SPL residual chronology and 2-month SPI for June-July derived from the 20.5–21°E/40–40.5°N grid cell (yellow) and all grids displayed in Fig. 4B (red).

Fig. S4. Inter-study comparison. A. The Mt Smolikas 2-month SPI June–July reconstruction (this study) shown together with a 3-month SPI June–August reconstruction from SW Romania (Levanic *et al.* 2012). B. Corresponding 31-year moving window correlations (1688–2010). C. Number of *Pinus nigra* samples. The vertical dashed line indicates 1758 CE when EPS passes the 0.85 threshold in the Romanian record.